Available online at www.sciencedirect.com

ScienceDirect

Ceramics International 40 (2014) 703–706

CERAMICS INTERNATIONAL

www.elsevier.com/locate/ceramint

Structure analysis and multiferroic properties of Zr^{4+} doped $BiFeO_3$ ceramics

Junjie Xie[a,b], Chude Feng[a], Xiuhong Pan[a], Yan Liu[a,*]

[a]State Key Laboratory of High Performance Ceramics and Superfine Microstructure, Shanghai Institute of Ceramics, Chinese Academy of Sciences, 1295 Dingxi Road, Shanghai 200050, China

[b]University of Chinese Academy of Sciences, Beijing 100039, China

Received 21 May 2013; received in revised form 15 June 2013; accepted 17 June 2013
Available online 21 June 2013

Abstract

Zr^{4+} doped multiferroic ceramics samples $BiFe_{1-x}Zr_xO_3$ ($x=0$, 0.02, 0.04, 0.06, 0.08, 0.10) were prepared by a solid state reaction method and characterized by X-ray diffraction and X-ray Absorption Fine Structure analysis. X-ray diffraction analysis showed that the characteristic peaks of samples were shifted toward a lower angle with the increase of Zr^{4+} doping concentration. It indicated that the doped Zr^{4+} ions entered into the crystal lattice. The length of Zr–O bond was calculated based on the results of X-ray Absorption Fine Structure analysis. The abnormal dielectric constant near the Neel temperature of $BiFe_{1-x}Zr_xO_3$ indirectly demonstrated the coupling between magnetic and electric properties of $BiFe_{1-x}Zr_xO_3$. The Neel temperature of Zr^{4+} doped $BiFeO_3$ was ~20 °C lower than that of the undoped $BiFeO_3$. The Neel temperature of $BiFe_{1-x}Zr_xO_3$ will be different if the doping amount of Zr^{4+} is different. However, all the prepared samples are antiferromagnetic.

Keywords: B. X-ray methods; C. Ferroelectric properties; C. Magnetic properties; E. Functional applications

1. Introduction

Multiferroic materials have attracted great attention because of two reasons. One is the potential applications in multifunctional sensors, convertors and microelectronic devices [1,2]. The other is their interesting physical problems, for example, the coupling between magnetic order parameters and electric order parameters [3,4]. As other important multiferroic materials, $BiFeO_3$ possesses ferroelectricity, anti-ferromagnetism and ferroelasticity [5]. Furthermore, $BiFeO_3$ is the only single-phase multiferroics, which has both Curie temperature (T_C, 1103 K) and Neel temperature (T_N, transition temperature from anti-ferromagnetism to para-magnetism, 643 K) above room temperature [6]. It is a good candidate for making lead-free ferroelectric memory devices due to its large spontaneous polarization (P_S, 88–100 μC/cm^2) [5] and high T_C [7,8]. However, its main drawback, the relatively high leakage current, impedes its further applications. The leakage current is caused by oxygen vacancies and Fe^{2+} in $BiFeO_3$. Oxygen vacancies come from the evaporation of Bi, and Fe^{2+} comes from the reduction of Fe^{3+}[9].

Although the impurity phases are inevitable in $BiFeO_3$ ceramic materials prepared by the solid state reaction method [6], it has been demonstrated that there is no correlation between the impurity phase intensity in XRD patterns and the leakage current [10–12]. Many methods have been tried to decrease the leakage current of $BiFeO_3$, such as aliovalent-ion-doping [9], rapid liquid phase sintering [12], thin film, etc. [7,13,14]. As for $BiFeO_3$ ceramics samples prepared by the solid state reaction method, doping is a main and convenient approach to decrease the leakage current. Decrease in the leakage current of Zr^{4+} doped $BiFeO_3$ prepared by the solid state reaction method was reported previously and the enhanced properties could be attributed to the change in the conduction mechanism and the competition of two different charge-compensation ways [15]. In this paper, the further discussions on Zr^{4+} doped $BiFeO_3$ prepared by the solid state reaction method will be carried out, such as the differences between Fe–O and Zr–O bond, and the resultant effect on the dielectric and magnetic properties.

2. Experiments

$BiFe_{1-x}Zr_xO_3$ (BFZO, $x=0$, 0.02, 0.04, 0.06, 0.08, 0.10) samples were prepared by a solid state reaction method.

*Corresponding author. Tel.: +86 21 52414821; fax: +86 21 52413903.
E-mail address: liuyan@mail.sic.ac.cn (Y. Liu).

0272-8842/$ - see front matter © 2013 Elsevier Ltd and Techna Group S.r.l. All rights reserved.
http://dx.doi.org/10.1016/j.ceramint.2013.06.058

The analytical purity regents of Bi_2O_3, Fe_2O_3 and ZrO_2 were mixed in a stoichiometric ratio with 3% (mol) extra Bi_2O_3 considering its evaporation. The mixture was milled for 24 h and then calcined in the air at 600 °C for 2 h. Then the calcined powder was milled again and pressed into pellets with 15 mm diameter and 2 mm thickness at the pressure of 135 MPa. The pressed pellets were sintered at 820 °C in the air for 50 min in an alumina crucible. After sintering, the samples with the crucible were immediately taken out from the furnace.

X-ray diffraction (D8 Advance) with CuKα_1 was used to analyze the phase of BFZO. X-Ray Absorption Fine Structure (XAFS) analysis was carried out with BL14W1 beam line in Shanghai Synchrotron Radiation Facility (SSRF). Ifeffit software was used for XAFS data processing. For the electric properties measurement, the as-sintered BFZO pellets were well polished as thin as 1 mm, and silver paste was pasted on the both sides as the electrodes. Agilent 4284A Precision LCR Meter was used to measure the dielectric properties. Magnetic properties were measured by vibrating sample magnetometer (VSM, Quantum Design).

3. Results and discussions

Fig. 1 (a) shows the XRD patterns of BFZO samples. All the XRD patterns indicate that it is a typical rhombohedral structure. There are two kinds of impurities in the BFZO samples, which are $Bi_2Fe_4O_9$ and $Bi_{25}FeO_{40}$, according to the XRD results. The impurities are due to the decomposition of $BiFeO_3$ at 720–1040 K during the cooling process from the sintering temperature [6]. As a result, the impurities are inevitable in $BiFeO_3$ prepared by the solid state reaction method. Although there are a few impurity phase (≤10%) showed in the patterns, the electrical properties of samples would not be affected [10–12]. It is found that the typical diffraction peaks are shifted toward a lower angle in Fig. 1(b) and (c). It means that Zr^{4+} ions are entered into the crystal lattice. Because the radius of Zr^{4+} ion (0.72 Å) is larger than that of Fe^{3+} ion (0.65 Å)[16], the unit cell size of BFO would be distorted and enlarged when Zr^{4+} entered into the lattice. As a result, the diffraction peaks of BFZO samples in XRD patterns would be shifted toward a lower angle. For further analysis, the neighbor coordinate conditions of Zr^{4+} ions in BFZO will be investigated by XAFS.

Fig. 2 shows the variation of Fourier transformed XAFS spectra of Zr K edge vs. the neighbor interatomic distance. Due to the time limitation of XAFS experiment, the sample of $x=0.02$ is not tested. The corresponding original data of X-ray absorption spectroscopies of K edge of Zr^{4+} ions are depicted in the inset of Fig. 2.

The original XAFS data are processed with Ifeffit software (free download, http://cars9.uchicago.edu/ifeffit/) based on the following theory reported by Stern, Sayer, and Lytle in 1975.[17,18]

The origin XAFS data is the relationship between $\mu(E)$ and E,

$$\mu(E) \sim E \tag{1}$$

$\mu(E)$: absorption coefficient.

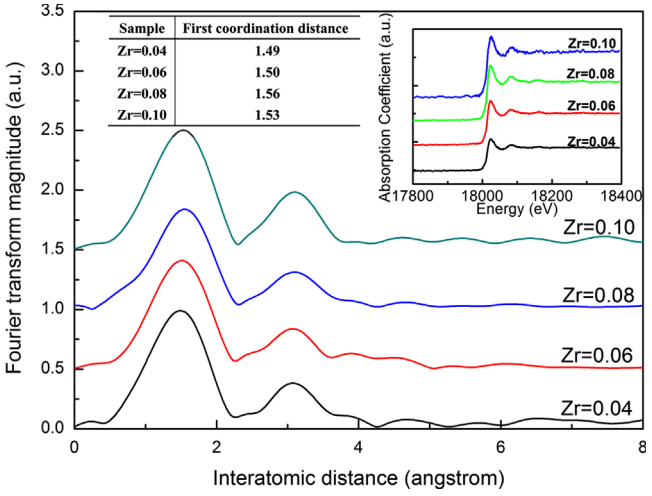

Fig. 2. Fourier transformed XAFS spectrum of Zr K edge.

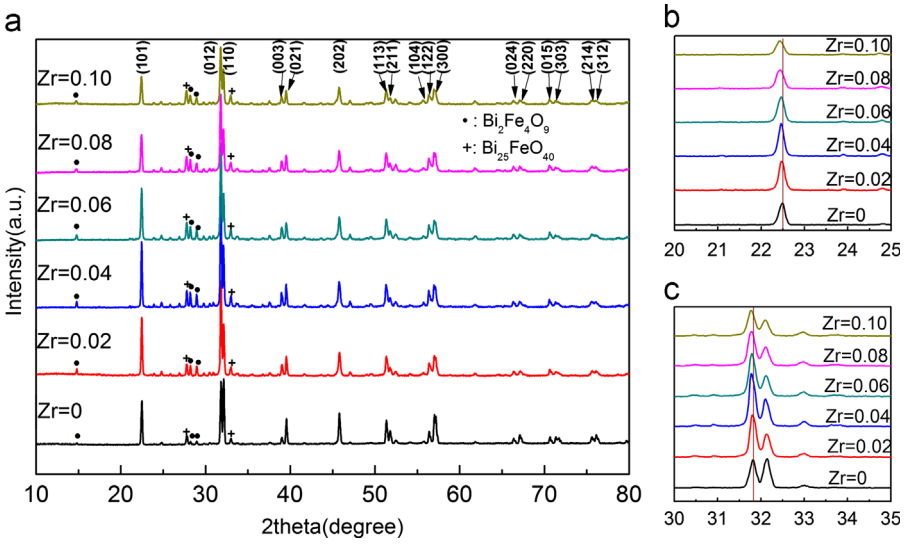

Fig. 1. The XRD patterns of BFZO.

Absorption coefficient must be nominalized and intrinsic absorption must be deducted, as following:

$$\chi(E) = \frac{\mu(E) - \mu_0(E)}{\mu_0(E)} \quad (2)$$

$\chi(E)$: nominalized absorption coefficient, $\mu_0(E)$: pre-edge baseline of absorption coefficient spectrum.

In the further analysis, the independent variables in Eq. (2) must be transformed from R space to k space, the relationship between R and k as following:

$$k = \frac{2\pi}{\lambda} = \sqrt{\frac{2m}{\hbar}(E - E_0)} \quad (3)$$

Because of the dumping of amplitude, the $\chi(E)$ must be multiplied by a weighting factor k^n, as for Zr, $n=2$. And then, the absorption coefficient Eq. (2) becomes

$$k^2\chi(k) \sim k \quad (4)$$

And then, the Eq. (4) can be transformed from k space to R space by Fourier transform; the transform equation is listed below:

$$\rho(R) = \frac{1}{\sqrt{2\pi}} \int_{k_{\min}}^{k_{\max}} \omega(k) k^2 \chi e^{-2ikR} dk \quad (5)$$

$$\omega(k) = \begin{cases} 0 & k < k_{\min} \\ \sin^2\left[\dfrac{\pi(k - k_{\min})}{2(k_2 - k_{\min})}\right] & k_{\min} < k < K_2 \\ 1 & k_2 < k < k_3 \\ \cos^2\left[\dfrac{\pi(k - k_3)}{2(k_{\max} - k_3)}\right] & k_3 < k < k_{\max} \\ 0 & k > k_{\max} \end{cases} \quad (6)$$

As for Zr^{4+} in BFZO, $k_2=2$, $k_3=10$.

At last, the absorption coefficient equation is transformed as following:

$$\rho(R) \sim R$$

R is the distance between central absorption atom and the coordinated atoms.

The first coordination peak can be observed clearly in Fig. 2. It corresponds to the nearest oxygen atoms around Zr^{4+} ion. There are two types of oxygen atoms coordinated to Fe^{3+} ions in pure $BiFeO_3$ and the bond lengths are 1.94 Å and 2.13 Å respectively.[19] However, this difference cannot be observed in BFZO. The inset table in Fig. 2 shows the length of Zr–O bond in BFZO. According to Coulomb's law, the bond length $r \propto Z_1Z_2/E_{bond}$, where Z_1, Z_2 are the valence of ions, and E_{bond} is the corresponding bond energy. For the Fe–O bond, the bond energy $E_{bond}=409$ kJ/mol[16], $Z_1=3$, and $Z_2=2$, so $Z_1Z_2/E_{bond}=0.0147$ (kJ/mol)$^{-1}$. For the Zr–O bond, the bond energy $E_{bond}=760$ kJ/mol [16], $Z_1=4$ and $Z_2=2$, so $Z_1Z_2/E_{bond}=0.0105$ (kJ/mol)$^{-1}$. As a result, the length of Zr–O bond is much shorter than that of Fe–O bond.

Fig. 3 shows the ε–T (dielectric constant–temperature) spectra of BFZO samples at 100 Hz. There is an abnormity in the spectra between 310 °C and 350 °C, which is corresponding to the transition from anti-ferromagnetism to para-magnetism at the

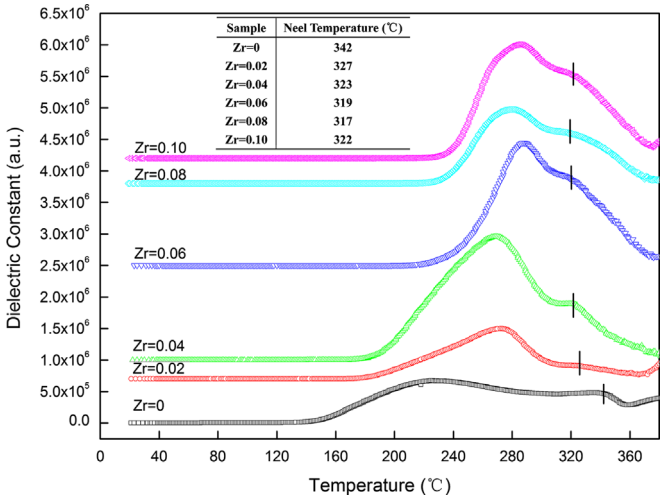

Fig. 3. The ε–T spectrum of BFZO at 100 Hz.

temperature T_N. The existence of impurity phases in BFZO results in the increase of the entropy of the system and the decrease of T_N [20]. Therefore, the T_N of undoped $BiFeO_3$ is slightly lower than that of the $BiFeO_3$ single crystal (643 K) [6].

It is well known that the magnet moment of Fe^{3+} arranges in a spatial modulating spiral structure. The superexchange interaction of Fe–O–Fe chain makes $BiFeO_3$ an antiferromagnetic material [21]. Dipole polarity makes a main contribution to the dielectric constant of dielectric materials at low frequency ($\leq 10^8$ Hz), and it is strongly related to the relative location between positive and negative charge center which can be affected by the length of Fe–O bond [22].

During the antiferromagnetism–paramagnetism transition, the rearrangement of Fe^{3+} magnetic moment will bring slight changes to the relative location between Fe^{3+} and O^{2-} due to the ferroelasticity of $BiFeO_3$ [23]. As a result, the relative location of positive and negative charge center changes and then dielectric constant will be affected. Since the magnetic moment ordering and dielectric constant are strongly correlated by Fe–O bond, the observed abnormal dielectric constant near T_N could be an indirect evidence for magneto-electric coupling in BFZO.

Because the net magnet moment of Zr^{4+} is zero, the doped Zr^{4+} ions in BFZO will disturb the spatial modulating spiral structure of Fe^{3+} magnetic moment. The relative location of positive and negative charge centers will be affected by doping as well. As a result, the T_N and dielectric constant are affected by Zr^{4+} doping. Due to the doping antimagnetic Zr^{4+} ions, the spiral ordering of Fe^{3+} magnetic moment is disturbed and the magnetic entropy increases. So T_N of Zr^{4+} doped samples decreased ~20 °C compared with that of the undoped $BiFeO_3$[20].

The magnetic properties of BFZO at room temperature are shown in Fig. 4. Almost all of the BFZO samples are antiferromagnetic according to the M–E plots. The doping amount of Zr^{4+} ions scarcely affects the magnetic type of BFZO samples although the T_N of Zr^{4+} doped $BiFeO_3$ decreased.

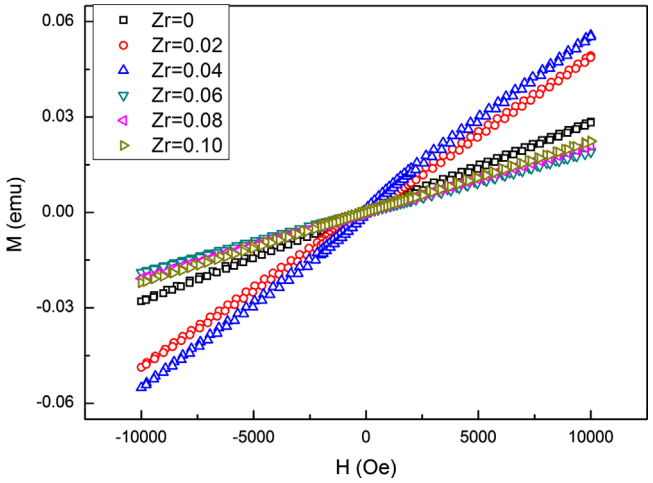

Fig. 4. The *H–M* plots of BFZO at room temperature.

4. Conclusions

Multiferroic $BiFe_{1-x}Zr_xO_3$ (BFZO, $x=0$, 0.02, 0.04, 0.06, 0.08, 0.10) samples were prepared by a solid state reaction method and characterized by XRD and XAFS. The analysis results reveal that the Zr^{4+} indeed entered into the crystal lattice of $BiFeO_3$, and Zr–O bond is much shorter than Fe–O bond. The magneto-electric coupling was indirectly observed in the dielectric constant–temperature spectra. The T_N of Zr^{4+} doped samples decreased ~20 °C comparing with that of the undoped $BiFeO_3$. All the as-prepared BFZO samples are antiferromagnetic.

Acknowledgment

This work is supported by the National Natural Science Foundation of China (51072209), the Innovation Fund of Shanghai Institute of Ceramics, CAS (Y17ZC11601G), and the Program of Scientific Equipment Development of Chinese Academy of Sciences (YZ201142). The authors thank beamline BL14W1 (Shanghai Synchrotron Radiation Facility) for providing the beam time.

References

[1] S.-W. Cheong., M. Mostovoy, Multiferroics a magnetic twist for ferroelectricity, Nature Materials 6 (2007) 13–20.
[2] W. Eerenstein, N.D. Mathur, J.F. Scott, Multiferroic and magnetoelectric materials, Nature 442 (7104) (2006) 759–765.
[3] M. Fiebig, Revival of the magnetoelectric effect, Journal of Physics D: Applied Physics 38 (8) (2005) R123–R152.
[4] N.A. Spaldin, M. Fiebig, Materials science: the renaissance of magneto-electric multiferroics, Science 309 (5733) (2005) 391–392.
[5] S.M. Selbach, T. Tybell, M.-A. Einarsrud, T. Grande, The ferroic phase transitions of $BiFeO_3$, Advanced Materials 20 (19) (2008) 3692–3696.
[6] S.M. Selbach, M.-A. Einarsrud, T. Grande, On the thermodynamic stability of $BiFeO_3$, Chemistry of Materials 21 (2009) 169–173.
[7] G.D. Hu, S.H. Fan, C.H. Yang, W.B. Wu, Low leakage current and enhanced ferroelectric properties of Ti and Zn codoped $BiFeO_3$ thin film, Applied Physics Letters 92 (19) (2008) 192905.
[8] H.W. Jang, D. Ortiz, S.-H. Baek, C.M. Folkman, R.R. Das, P. Shafer, Y. Chen, C.T. Nelson, X. Pan, R. Ramesh, C.-B. Eom, Domain engineering for enhanced ferroelectric properties of epitaxial (001) $BiFeO_3$ thin films, Advanced Materials 21 (7) (2009) 817–823.
[9] X. Qi, J. Dho, R. Tomov, M.G. Blamire, J.L. MacManus-Driscoll, Greatly reduced leakage current and conduction mechanism in aliovalent-ion-doped $BiFeO_3$, Applied Physics Letters 86 (6) (2005) 062903.
[10] T. Ito, T. Ushiyama, Y. Yanagisawa, R. Kumai, Y. Tomioka, Growth of highly insulating bulk single crystals of multiferroic $BiFeO_3$ and their inherent internal strains in the domain-switching process, Crystal Growth and Design 11 (11) (2011) 5139–5143.
[11] V.A. Khomchenko, V.V. Shvartsman, Crystal structure and magnetic properties of $Bi_{0.8}(Gd_{1-x}Ba_x)_{0.2}FeO_3$($x=0$, 0.5, 1) multiferroics, Journal of Physics D: Applied Physics 42 (4) (2009) 045418.
[12] Y.P. Wang, L. Zhou, M.F. Zhang, X.Y. Chen, J.M. Liu, Z.G. Liu, Room-temperature saturated ferroelectric polarization in $BiFeO_3$ ceramics synthesized by rapid liquid phase sintering, Applied Physics Letters 84 (10) (2004) 1731.
[13] T. Kawae, H. Tsuda, A. Morimoto, Reduced leakage current and ferroelectric properties in Nd and Mn codoped $BiFeO_3$ thin films, Applied Physics Express 1 (2008) 051601.
[14] H. Yang, H. Wang, G.F. Zou, M. Jain, N.A. Suvorova, D.M. Feldmann, P.C. Dowden, R.F. DePaula, J.L. MacManus-Driscoll, A.J. Taylor, Q.X. Jia, Leakage mechanisms of self-assembled $(BiFeO_3)_{0.5}$:$(Sm_2O_3)_{0.5}$ nanocomposite films, Applied Physics Letters 93 (14) (2008) 142904.
[15] J. Xie, Y. Liu, C. Feng, X. Pan, Preparation and characterization of Zr^{4+}-doped $BiFeO_3$ ceramics, Materials Letters 96 (1) (2013) 143–145.
[16] J.G. Speight, in: Lange's Handbook of Chemistry, McGRAW-HILL, New York, 2004.
[17] G. Bunker, Report on the International Workshops on Standards and Criteria in XAFS, in: Proceedings of the Sixth International Conference on XAFS, York, 1990.
[18] K. Lu, L. Ma, Analytica Chimica Acta 210 (1988) 143.
[19] J. Dhahri, M. Boudard, S. Zemni, H. Roussel, M. Oumezzine, Structure and magnetic properties of potassium doped bismuth ferrite, Journal of Solid State Chemistry 181 (4) (2008) 802–811.
[20] G.F. Dionne, in: Magnetic Oxides, Springer, New York, 2009.
[21] I. Sosnowska, T.P. Neumaier, E. Steichele, Spiral magnetic ordering in bismuth ferrite, Journal of Physics C: Solid State Physics 15 (23) (1982) 4835.
[22] P.J. Harrop, in: Dielectrics, Butterworths, London, 1972.
[23] F. Kubel, H. Schmid, Structure of a ferroelectric and ferroelastic monodomain crystal of the perovskite $BiFeO_3$, Acta Crystallographica Section B 46 (6) (1990) 698–702.